On the use of Tailored Permeable Surfaces for Turbulence Interaction Noise Control

Luke Bowen*, Alper Celik†, Mahdi Azarpeyvand‡
Faculty of Engineering, University of Bristol, BS8 1TR, UK

Carlos R. Ilário da Silva§
Embraer, Sáo José dos Campos, 12227-901, Brazil

Turbulence interaction noise reduction using porous leading edges has been investigated experimentally. The effect of having a porous leading edge on the aeroacoustic characteristics of an additive manufactured NACA 0012 profile were investigated using leading edges manufactured from commercial metal foams and leading edges which are additive manufactured at a Reynolds number of 2.6×10^5. The first 10% of the airfoil is interchangeable with the multiple porous cases tested. The additive manufactured NACA 0012 profile shows a good agreement between experimental pressure coefficient values and XFoil predictions, and the interaction noise radiates well above the background of the jet. The turbulent inflow is generated by a grid placed within the contraction nozzle. The effect of the investigated leading edges are quantified in terms of the radiated far-field noise and are compared to the results of a solid leading edge. It showed that far-field noise was reduced for low frequency in all cases, although some suffer a larger high frequency penalty than others. A porous leading edge with a cover appears to abate this increase in high frequency noise and show little detrimental effect to the hydrodynamic field of the solid part of the airfoil at low angles of attack.

I. Nomenclature

C	=	Inertial loss term [m^{-1}]
c	=	Chord [m]
d	=	Grid Bar Diameter [mm]
f	=	Frequency [Hz]
k_e	=	Wavenumber range of energy-containing eddies [-]
k_x	=	Streamwise wavenumber [-]
m	=	Mesh size [mm]
p	=	Pressure [Pa]
p'	=	Pressure fluctuation [Pa]
p_{ref}	=	Reference pressure $2x10^{-5}$ [Pa]
PSD	=	Power spectral density [dB/Hz]
Re	=	Reynolds number [-]
t	=	Thickness [mm]
U_∞	=	Free-stream velocity [m/s]
u	=	Streamwise velocity fluctuation [m/s]
V	=	Volume [m^3]
Γ	=	Gamma function [-]
κ	=	Porosity [-]
Λ	=	Integral Length Scale [mm]
ρ	=	Fluid density [kg/m^3]
σ	=	Solidity ratio [-]

*Ph.D Student, Department of Mechanical Engineering, luke.bowen@bristol.ac.uk
†Postdoctoral Research Associate, Department of Mechanical Engineering, alper.celik@bristol.ac.uk
‡Professor of Aerodynamics and Aeroacoustics, Department of Mechanical Engineering, m.azarpeyvand@bristol.ac.uk
§Challenge Owner in Electrifying Aviation, Embraer, Sáo José dos Campos, Brazil, carlos.ilario@embraer.com.br

υ = Darcian Velocity [m^3/s]
ϕ_{pp} = Power spectral density of the pressure fluctuation [dB/Hz]
ϕ_{uu} = Power spectral density of the streamwise velocity fluctuation [dB/Hz]
φ = Porosity [-]
ω = Angular frequency [rad/s]

II. Introduction

Turbulence interaction noise is an ever-increasing factor in the drive towards more sustainable methods of propulsion. The rotating motion of the fan causes a highly rotational, turbulent flow and to increase the efficiency the flow is then straightened by stator vanes. The flow from the fan contains turbulent structures that interact with the leading edge of the stator, causing fluctuating pressure forces on the surface of the airfoil, which is the noise generation mechanism of interest. This can be simplified to the interaction between a turbulent inflow, generated by a grid, and the interaction of an airfoil. The nature of this interaction noise is such that the geometry of impingement is an important factor, as is the qualities of impingement itself. When the structures are large, making the leading edge appear sharp in comparison the leading edge, the full efficiency of this noise generation can be achieved. To understand the effect of changing the leading edge structure with the same geometry, the turbulent structures must be larger than the leading edge radius. Turbulence interaction noise is a subject that has been of large social interest for some time and historically has been well studied. Paterson and Amiet [1] originally proposed the idea of turbulence impingement as low frequency dominating noise radiation, considering the scale of turbulence is large. Amiet went on to propose a model [2] which can predict the interaction noise by first using linearized theory to calculate the aerodynamic response of the incident gust on the airfoil; then calculating the unsteady lift propagation to the acoustic far-field accounting for scattering and mean flow effects. Moreau and Rodger [3] studied the effects that angle of attack has on noise generation in turbulent flow and showed there is almost no dependency angle of attack. Devenport et al. studied the effects of real airfoils in turbulence [4] and concluded that although angle of attack has a strong effect on the airfoil response function, it only has a small effect on noise generation. As turbulent inflow conditions are an important factor, this was extensively studied by Hutcheson et al. [5] consisting of a host of different inflow conditions and geometries, finding that as length scale and intensity increased this uniformly increased the spectral levels. As the geometry is an important factor in the noise generation there have been many studies subject to this [3, 4, 6–8], all finding that the airfoil geometry does in fact alter the noise generation in turbulent flow.

Active [9, 10] and passive [11–16] noise control techniques have shown in many instances that they are effective methods of noise reduction when well implemented into trailing edges. Turbulence interaction noise has previously shown that it can be reduced by using passive leading edge treatments, and the use of serrations has had an increasing level of interest in recent years [17–21]. Interaction noise reduction with porous materials has also been the subject of many previous studies and shows a viable method for a correctly implemented solution to the reduction of noise generated at the leading edge. Rodger et al. [22, 23] used grid generated turbulence to measure the effect that a steel-wool filled NACA 0012 had on noise radiation and showed a maximum of 5dB of noise reduction is achievable from a sub-optimal approach. Geyer and Sarradj have carried out multiple studies on porous airfoils [24–26], the first study on the effect of fully porous airfoils in turbulent flow [24]. The study focused on changing porous properties of airfoils to assess the acoustic benefit, a reduction in noise for most cases was found at the detriment to the overall hydrodynamic performance of the airfoil. Further works have showed the potential of porous materials for noise reduction [11, 27–30], but a common conclusion is found that better understanding of the mechanisms and flow interaction is needed to optimise the implementation of porous materials for the noise abatement. Zamponi et al. [31] conducted boundary layer measurements around a porous airfoil to better understand the flow conditions. As with previous studies [11, 12] they found that the porous material will decrease the low frequency noise contribution and increase at high frequency, suggested to be surface roughness [12].

This study aims to offer an alternative to off-the-shelf porous metal foams, to show a degree of control over the porosity and permeability and to demonstrate the performance of tailored permeable surfaces that can optimize the implementation of a porous leading edge. The study looks at various leading edge structures and compares them to already extensively tested porous metal foams and assess their performance of radiation to the far-field. Coefficient of pressure measurements were made to assess the effect of the hydrodynamic field and unsteady surface pressure measurements were also made to understand the effects of the porous material on the mid-chord and trailing edge of the airfoil.

III. Measurement setup

A. Wind tunnel and model

The experiments were performed in the University of Bristol Aeroacoustic Facility, which is a closed-circuit, open-jet anechoic wind tunnel, shown in Fig. 1. The chamber is anechoic down to 160Hz with physical dimensions of 6.7 m x 4.0 m x 3.3 m, the nozzle has an area of 500 mm x 775 mm which allows for a steady operation from 5 m/s to 45 m/s and a normal turbulence intensity level below 0.2% [32]. Far-field noise measurements were made using 23 1/4 inch GRAS 40PL microphones which have a large dynamic range and an upper limit of 142dB, covering a frequency range between 10 Hz and 20,000 Hz. 23 of these microphones were arranged on to a far-field array arc allowing measurement between 35° and 150° polar angles at a distance of 1.75 m from the leading edge of the airfoil.

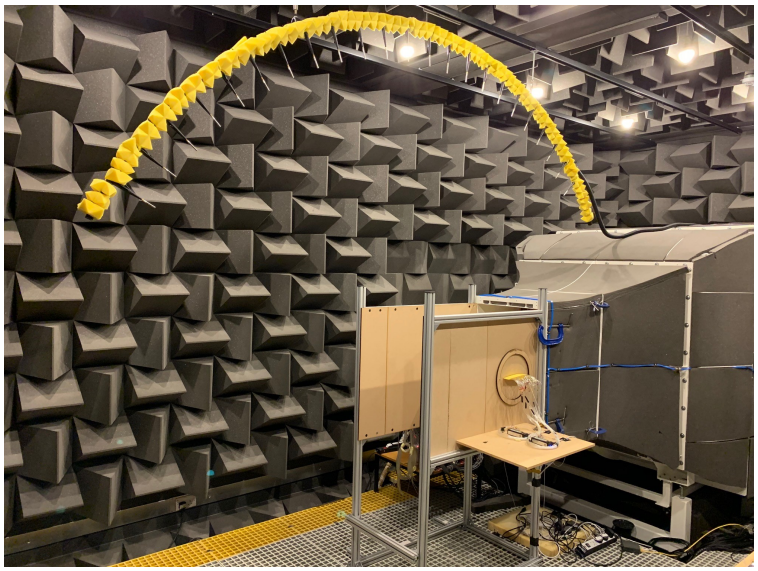

Fig. 1 Picture of experimental set up within aeroacoustic wind tunnel at University of Bristol.

The NACA 0012 airfoil was designed and manufactured at the University of Bristol. It was 3D printed by an Ultimaker S2 printer and brass tubes were installed using a 2 part epoxy resin and smoothed into the surface. It has a chord of 0.2 m and a span of 0.6 m. The airfoil has been highly instrumented to fully capture the aerodynamic and aeroacoustic phenomena. Instrumentation included 56 pressure taps for the measurement of the hydrodynamic field around the airfoil, and 56 taps for surface pressure fluctuation measurement. The surface pressure taps were connected in a remote sensing configuration using Panasonic WM-61A microphones [33]. Both the pressure taps and the surface pressure taps were drilled with 0.4mm pinholes to avoid pressure attenuation at high frequencies. All microphones were calibrated in both magnitude and phase referenced to a single GRAS 40PL microphone, which was calibrated using a GRAS 42AA pistonphone calibrator. Static pressure measurements were taken from two Chell MicroDaq-32 pressure acquisition systems and were sampled for 32 seconds at 500 Hz.

B. Porous leading edges

Figure 3 illustrates a schematic of the airfoil, and its first 10% of the chord which is interchangeable and can be exchanged between a solid, instrumented leading edge and various porous leading edges. A range of porous materials were tested which encompassed both metal foams and tailored permeable materials. Following the method previously implemented [11–13] the porosity and permeability of these structures needs to be determined. Porosity is defined by

$$\varphi = V_V / V_T, \tag{1}$$

where V_V is the volume of the void and V_T is the total volume of the sample. By measuring the pressure drop across the sample, and using the Dupuit-Forchheimer equation the permeability of the sample can be determined as previously measured [11, 12]. The measured pressure drop Δp is used in the equation

$$\Delta p / t = \mu / \kappa \upsilon_D + \rho C \upsilon_D^2, \tag{2}$$

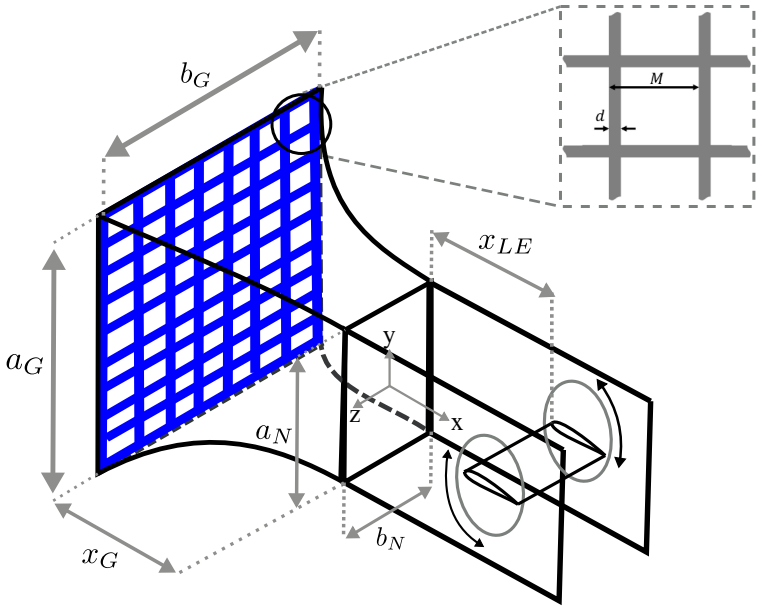

Fig. 2 A schematic of the set up and the geometry that defines the turbulence grid used.

where κ is the permeability coefficient, t is this thickness of the sample, ρ is the density of the fluid, C is the inertial loss term and υ_D is the Darcian Velocity which is defined as the volume flow rate divided by the cross-sectional area of the sample.

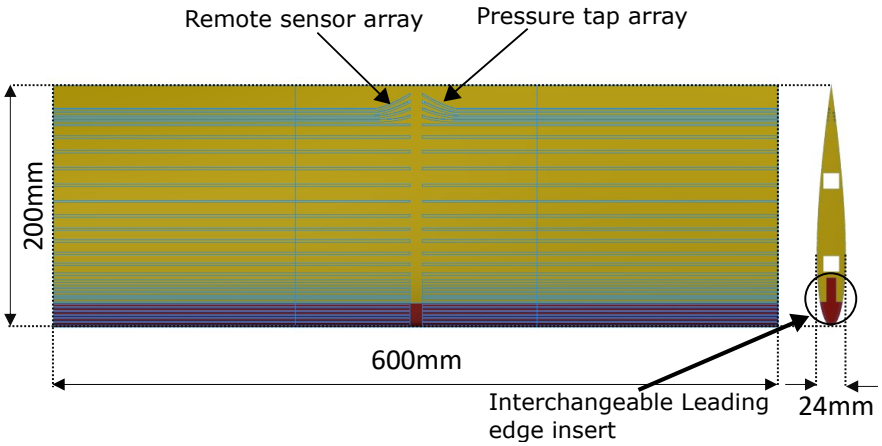

Fig. 3 Schematic of 3D printed NACA 0012 airfoil.

1. Metal Foam Leading Edges

The two metal foams used for this study were of 25 and 45 PPI (pores per inch). Sheets of this metal foam were cut using electrical discharge machining (EDM) into the shape of the leading edge of the airfoil, shown in Fig. 4. The porosity and permeability values were previously measured using X-Ray Computed Tomography (CT) Scanning and the permeability test rig over a wide range of Darcy velocities. The values of porosity were previously found to be 90.92% and 85.37% and permeability values of $8.2\text{x}10^{-8}$ m^2 and $2.1\text{x}10^{-8}$ m^2, respectively [11, 12].

2. Tailored permeable leading edges

Six other tested cases were tailored permeable structures and designed using CAD and depicted in Fig. 5. Three of the cases used mathematically designed surfaces, a coarse construction and two fine constructions, with and without covers. Two cases were lattice type structures, with and without covers. One case was based on patterned sine waves and extruded from a cube. This cube was patterned and cut to the shape of the leading edge. All were 3D printed and tested. Figure 5 shows their base feature, and the overall structure. The three mathematically designed surfaces were Schwarz-P surfaces which are Triply-Periodic Minimal Surfaces (TPMS) were first describe by Schwarz [34, 35]. This surface is generated from the control of the equation

$$\cos(lx) + \cos(ly) + \cos(lz) = a, \tag{3}$$

where l is used to define the unit length, and a is a constant that controls the porosity.

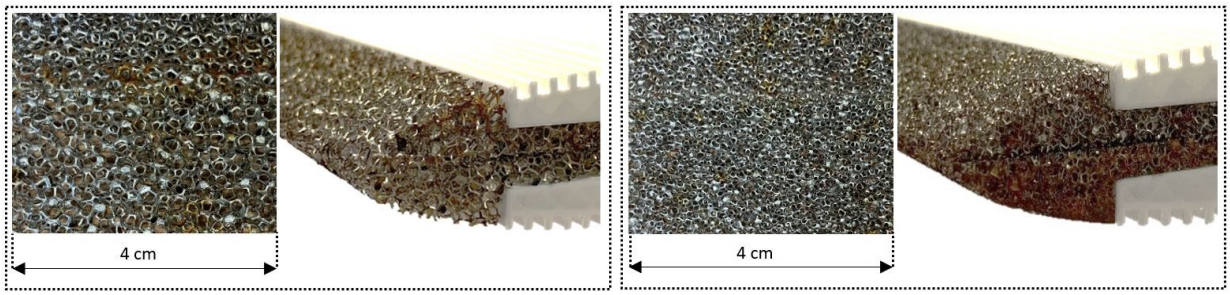

Fig. 4 Metal foam porous leading edges, a) 25 PPI (P1 case), b) 45 PPI (P2 case)

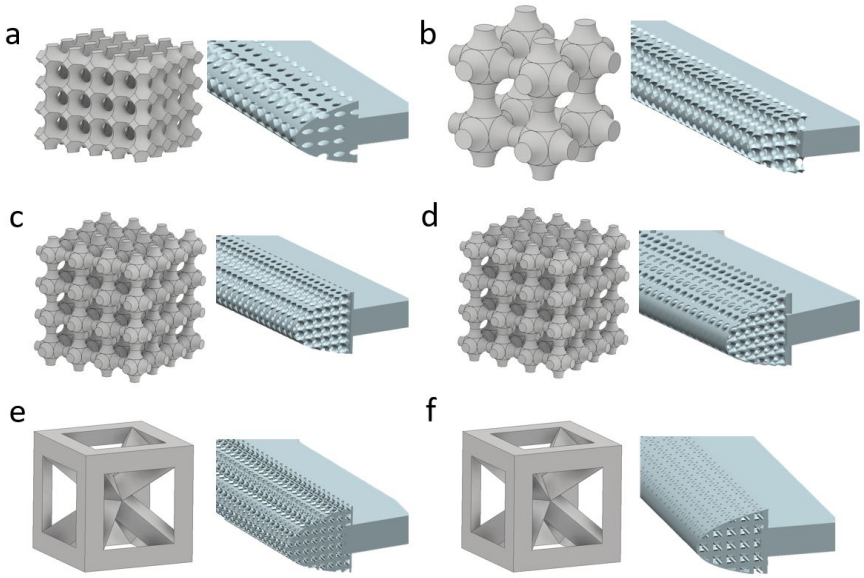

Fig. 5 Tailored permeable leading edges and their base features. (a) Sinewave based structure (P3), (b) Coarse Schwarz-P structure (P5), (c) Fine Schwarz-P structure (P7), (d) Fine Scharwz-P structure with cover (P8), (e) lattice structure (P4), (f) Covered lattice structure (P6).

C. Turbulence grids

To generate the incoming turbulence, a turbulence grid was required to be designed. A separate study has been carried out to characterise the effects of geometric changes on turbulence grids in an aeroacoustic wind tunnel. For this

study the geometric parameters defined by Fig. 2 are bar diameter, d = 19 mm and the mesh size, M = 100 mm. The ratio between the cross-sectional area of the point at where the grid is mounted and the nozzle exit is represented by $(a_G \cdot b_G)/(a_N \cdot b_N)$ and is 4.4. The solidity ratio of the grid, σ is also used to quantify the expected pressure drop across the grid and is defined by $\sigma = d/M(2 - d/M)$. Figure 2 relates the equation to the geometric properties of the grid that defines σ, which for this grid is 0.35.

Before the measurement of the interaction noise the turbulent flow was characterised using Constant Temperature Anemometry Hot-wire. A Dantec 55P16 single hot-wire probe was used to measure the streamwise component of velocity, which was operated using a Dantec Streamline Pro system with CTA91C10 module and the probe was calibrated using a Dantec 54H10 calibrator. The measurements were sampled at a rate of 2^{15} Hz for 32 seconds using a National Instruments PXIe-4499 module mounted in a Nation Instruments PXIe-1026Q chassis. The grid generated turbulence intensity of the flow was found to be 4.3% with an Integral Length Scale of 0.019 m at the point of where the leading edge would be positioned. The tests were carried out at the free-stream velocity of U_∞ = 20 m/s, corresponding to the chord-based Reynolds Number of Re= 2.6 x 10^5. To ensure the grid was suitable for direct far-field measurement this was checked against far-field background noise of the tunnel with no grid present. As shown in Fig. 6, far-field noise data collected at 20 m/s demonstrates that the self noise from the grid does not affect the far-field noise.

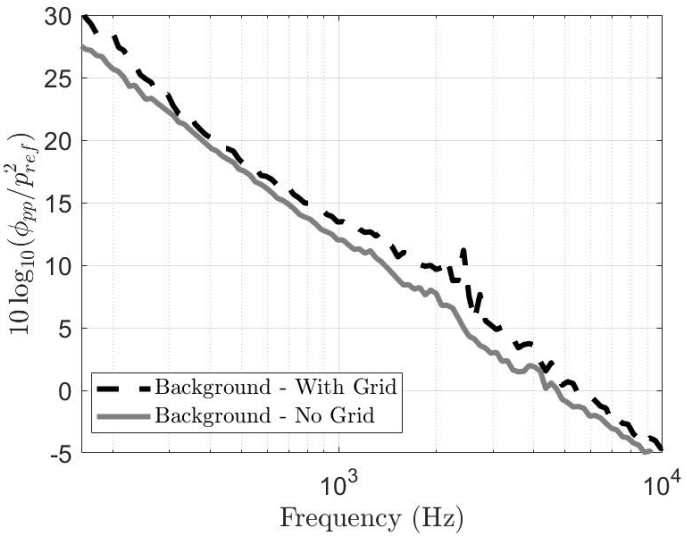

Fig. 6 Background noise of aeroacoustic wind tunnel with and without a turbulence grid.

IV. Results and Discussion

A. Validation of 3D printed NACA 0012

Manufacturing an airfoil using rapid prototyping technology followed by instrumenting the airfoil for both static pressure measurement and near-field unsteady pressure measurement is a relatively new process to the University of Bristol. To ensure that the geometry of the airfoil was accurate, and the introduction of the sensor arrays was non-intrusive, the measurements of static pressure were validated against XFoil. Cases for both laminar and turbulent flow were conducted for XFoil prediction, which was controlled by the "NCrit" parameter which controls the free transition parameters and the Reynolds number was matched to that of the test being carried out, Re= $2.6x10^5$. Laminar cases were conducted with and without a trip located at 20% of the chord. All the aforementioned XFoil predictions were compared to the experimental data, although for brevity, only the laminar case will be shown, however all cases show good agreement across the tested cases. Figure 7 displays the calculated coefficient of pressure data and the computed XFoil data for the same flow conditions, which shows a good agreement between the experimental data collected and computed values over a range of angles. The anechoic wind tunnel is an open jet wind tunnel and the geometric angle of attack is not the true attack experienced by the airfoil as the jet core will be deflected by the airfoil at an angle of inclination. Due to this deflection, a correction is required between the geometric angle of attack and the

true angle. The correction is achieved by comparing the measured experimental pressure distribution with a computed pressure distribution from XFoil for multiple angles until a match is found. A correction multiplier of 0.75 is required to be applied to the geometric angle to gain the true angle experienced in the flow. This was found to be valid for all angles less than 10°. The good agreement between the XFoil prediction and the experimental data suggests the rapid prototyping and instrumentation method to be appropriate for this study and an accurate representation without intrusion to the flow.

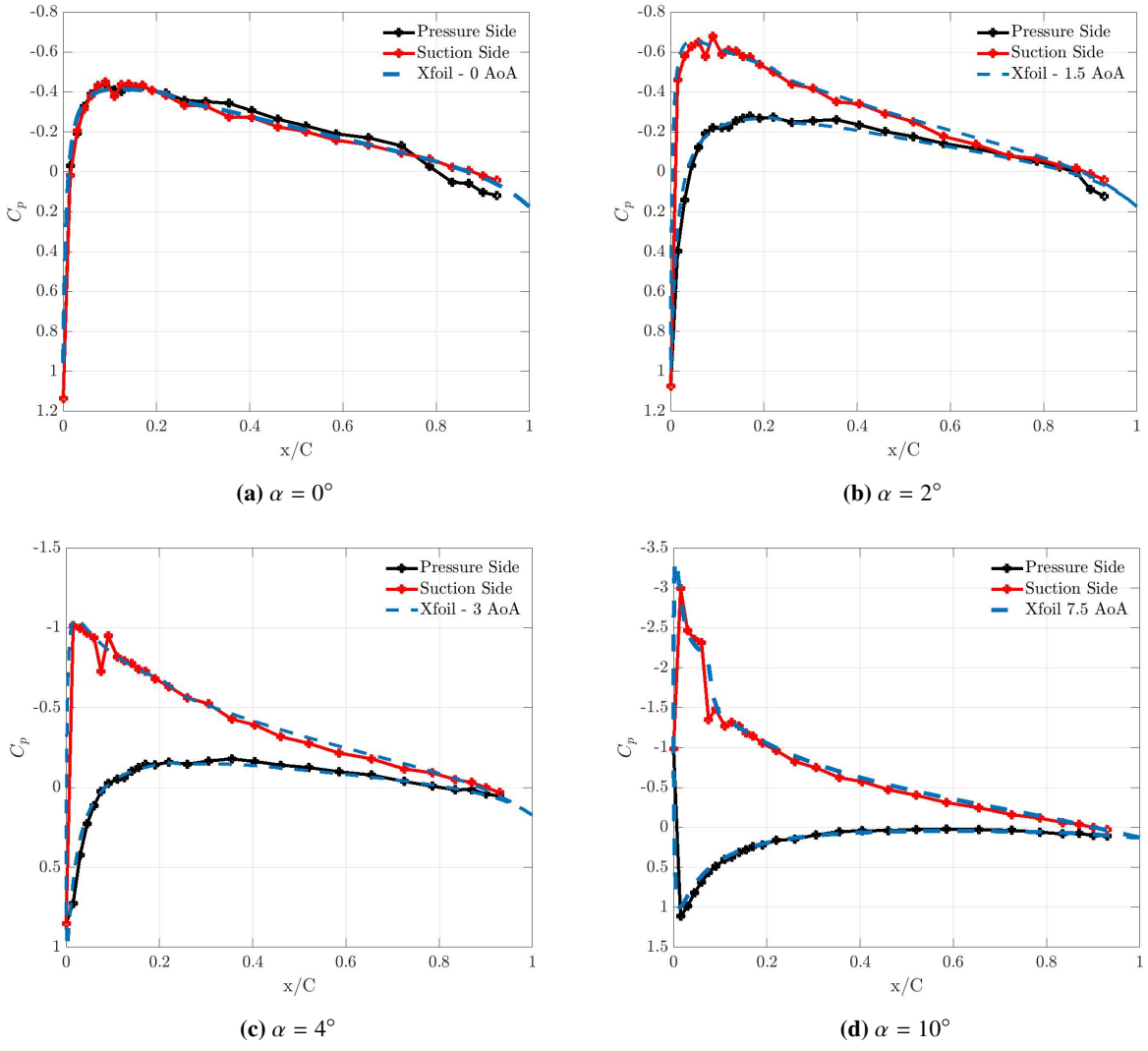

(a) $\alpha = 0°$ **(b)** $\alpha = 2°$

(c) $\alpha = 4°$ **(d)** $\alpha = 10°$

Fig. 7 Coefficient of pressure on the upper and lower surface of the airfoil, and the XFoil validation at various angles of attack.

B. Far-field noise

This section displays the Power Spectral Density (PSD) of the radiated noise that was recorded at the far-field above the airfoil. The microphone at 90° on the array was positioned 1.75 m directly above the leading edge of the airfoil. It is calculated using $PSD = 10 \cdot \log_{10}(\phi_{pp}/p_{ref}^2)$, where ϕ_{pp} is the power spectral density of the measured acoustic pressure and p_{ref} is the reference pressure of 20μPa. The directivity of the far-field noise PSD is also considered at various selected frequencies, to assess how these contribute to the overall radiated noise. Further to this, the total

radiated noise and its directivity is analysed through the overall sound pressure level which was calculated by

$$OASPL = 10 \cdot \log_{10}\left[\frac{\int \phi_{pp}(f)df}{p_{ref}^2}\right], \tag{4}$$

integrating the energy spectrum with respect to frequency, between 160 Hz to 20 kHz. The far-field noise assesses the changes in noise emission between metal foams and the solid case as well as the tailored permeable structures. All cases presented are for a freestream velocity of $U_\infty = 20$ m/s and the results are only presented for $\alpha = 0°$.

1. At 90° *above leading edge*

The performance of the metal foam leading edges compared to the solid baseline case is presented in Fig. 8. The results of the solid baseline suggests that the majority of the noise generated in interaction noise is below 1000 Hz for this case, and above 1000 Hz the radiated noise is within 5 dB of the normal background noise of the grid. Over the frequencies presumed to be caused by interaction noise, both materials exhibit potential to reduce noise. Between 250 and 700 Hz both metal foam leading edges show at least a 2 dB decrease in PSD, and between 700Hz and 1000Hz the performance appears to be consistent with the solid base line. However, for frequencies above 1000Hz, a penalty is incurred, which is potentially due to the surface roughness of the material. In previous studies roughness has been shown to increase noise at high frequencies [12], but for leading edge turbulence interaction this is yet to be confirmed. Overall, it appears that P2 out-performs P1 in its ability to reduce noise for frequencies less than 1000 Hz. Above 1000 Hz the best performing metal foam leading edge is less clear, as P2 has more of an increase over P1 around 2000 Hz, but the same spectral shape. Both P1 and P2 have a common peak at 2800 Hz which suggests it could be caused by the geometry in the addition of the porous materials as it is not evident in the solid case. Beyond this peak, P1 shows more of a noise increase over P2 with a value of nearly 5 dB more.

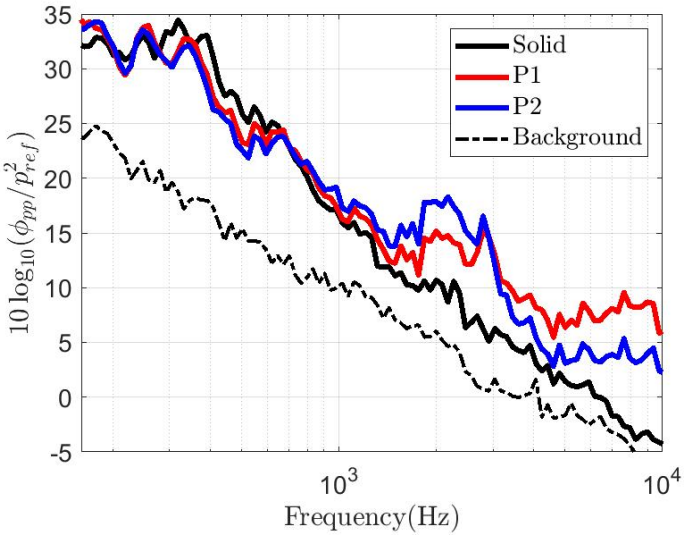

Fig. 8 Comparison of far-field noise between solid leading edge and metal foams.

Figure 9 describes the performance across the measured frequencies for two of the additive manufactured tailored porous materials. This comparison shows the same overall porous structure, however a thin layer was printed over the porous structure to provide a smoother surface. Again, a similar trend was observed as the metal foam leading edge for the case of turbulence interaction noise but with noticeable changes in performance. Between 160 Hz and 1000 Hz there is no increase over the baseline for the additive manufactured leading edges which should lead to an overall greater noise reduction over the metal foams leading edges. Further to this, the lower frequencies offer a greater reduction of interaction noise, up to 5 dB reduction is achieved compared to the baseline. The largest reduction in the noise is caused between 200 Hz and 700 Hz for both P7 and P8. Between 450 and 700 Hz the covered P8 structure achieves further noise reduction compared to P7. Between 1000 Hz and 3000Hz, the broadband hump which was observed in the metal

foam case appears to not be created by the additive manufactured leading edges, and both materials closely match the solid leading edge in these frequencies. However, above 3000 Hz it is evident that there is a generation of broadband noise in excess of the solid leading edge. Although there is an increase in both P7 and P8, P7 generates significantly more noise than P8 between 4000 Hz and 7000 Hz. This increase could be due to the surface roughness of the structure, as the introduction of a cover for the same materials appears to dampen the high frequency noise increase. Again, this needs to be confirmed for the case of porous materials in leading edge interaction noise.

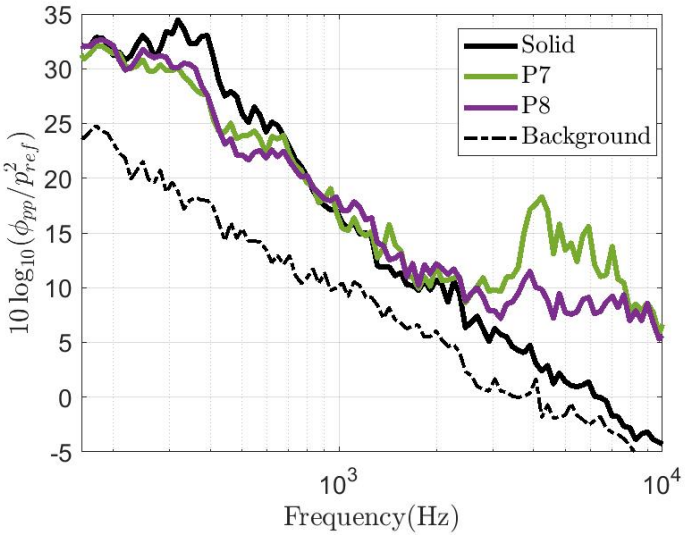

Fig. 9 Comparison of far-field noise between solid leading edge and 3D printed structures.

2. Far-field noise directivity

The overall sound pressure level gives the true indication of whether a noise reduction is achieved as it is the integration across the full spectrum of noise recorded. It includes both the reduction exhibited at low frequencies as well as the high frequency noise increase and the total gives the indication of whether an overall reduction is achieved. Figure 10 displays the overall sound pressure level between the polar angles 55° and 130°, for both the metal foam leading edges and the tailored structures leading edges which are compared with the solid baseline. In the case of the metal foams, Fig. 10a, there is a small measured reduction in the radiated sound for polar angles up to 105°, where P2 shows an increase over the baseline and P1. Apart from the increase, the directivity pattern remains unchanged with a small reduction overall. Figure 10b displays the OASPL directivity for the tailored structures which showed a larger reduction compared to the metal foams, with an exception of P7 between polar angles of 55° and 70°. Between these angles, P7 has an increased OASPL compared to the baseline and P8. The covered P8 leading edge shows a reduction over the solid leading edge across the full set of polar angles measured, and the greatest reduction in interaction noise compared to the baseline case.

To understand how individual frequencies contribute to the noise reduction, and if the directivity of the radiated noise is affected at these frequencies, the individual values of the frequency were plotted at each microphone location on the far-field arc. Figure 11 was constructed to illustrate the noise reduction at individual frequencies over the range that contribute most to the overall noise reduction from the porous leading edges. 200 Hz through to 700 Hz are displayed in intervals of 100 Hz and show the directivity pattern of each contributing frequency. At 200 Hz, solid, P1 and P2 leading edges have the same emission of noise and matching directivity pattern suggesting that the porous material has no effect at this frequency. Moving to 300 Hz, a clear reduction in noise is observed for both P1 and P2, with the latter being more effective. The overall directivity pattern remains unchanged, although the magnitude is reduced by the porous materials. The greatest contribution to the reduction of noise comes at 400 Hz, where both P1 and P2 are substantially lower than the solid baseline case. Again, the overall directivity pattern is similar but as the polar angles reduce to below 70° there is less of a noise reduction from P1 and P2 leading edges. A very different directivity pattern is exhibited at 500 Hz with the appearance of multiple lobes, but again the patterns match between the different materials. The results

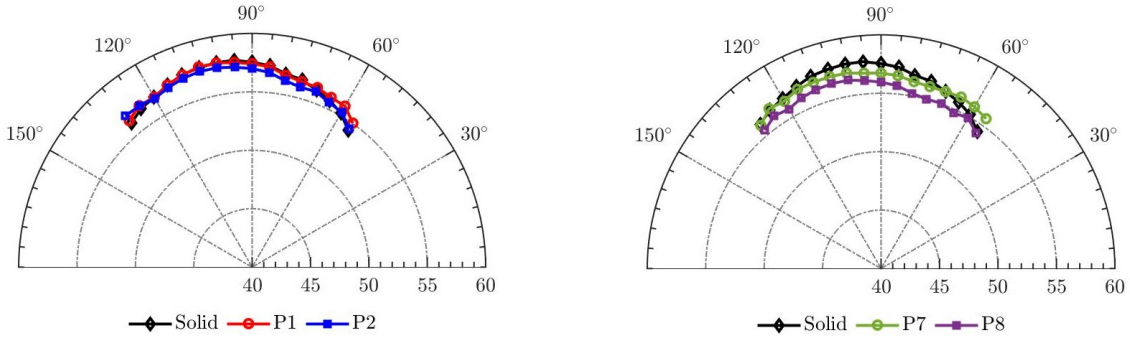

(a) Metal foam leading edges **(b) Tailored structures leading edges**

Fig. 10 Directivity of the overall sound pressure level of the radiated sound by both the metal foam and the tailored structure leading edges compared with the solid baseline.

have shown that P1 and P2 offer a reduction in noise for polar angles greater than 70° and P2 remains the most effective leading edge of the metal foams that were tested. At 600 Hz the reduction in noise starts to diminish due to the porous leading edges although a reduction is still evident. A reduction is evident at all angles for P1 and P2 leading edges, however it is more pronounced at polar angles above 90°. By 700 Hz, as seen in Fig. 8, there is no reduction in far-field noise. The noise emission from P1 and P2 matches the solid case, in both magnitude and directivity. Overall, P1 and P2 offer a reduction in far-field noise emission over these frequencies, and although they generally follow the same pattern of directivity over the polar angles that were measured, more reduction is seen for angles above 70°.

The directivity pattern over selected frequencies for the additive manufactured leading edges is displayed in Fig. 12, and although the magnitude is reduced in these cases the overall trend is similar to that of the metal foam leading edges. For the additive manufactured leading edges the magnitude of noise reduction is greater over the selected frequencies, although the main reduction is also above 70° polar angle. The shape of the directivity in each frequency that is displayed matches between the solid, P7 and P8 leading edges suggesting that the noise reduction doesn't majorly affect the directivity of the radiated sound, apart from the lower polar angles measured. The greatest reduction is at 400 Hz, and P8 shows the greatest reduction. Unlike the metal foams, P7 and P8 show reduction in the generated noise at 700 Hz. Overall, it seems that the most promising candidate tested for noise reduction in leading edge interaction noise in an additive manufactured leading edge with a smoothing cover.

C. Aerodynamic performance of tailored structures

The most effective porous case in terms of far-field noise reduction is evidently the covered fine Schwarz-P structure, P8. To assess whether this benefit is detrimental to the aerodynamic performance, the coefficient of pressure, and the root mean square (rms) values of the coefficient of pressure were compared to the solid case. Although no direct comparisons or conclusions can be raised for the leading edge area of the porous structures, the downstream effect for the solid part of the airfoil can be compared between the cases. Figure 13 depicts the coefficient of pressure data for both metal foams P1 and P2, and both additive manufactured leading edges P7 and P8 which are compared to the baseline solid case. For both Figs. 13a and 13b, the pressure and suction side measurements collapse on top of of each other as the airfoil is symmetric and has a 0° angle of attack. For the $C_{p_{rms}}$ case, the suction size is represented by the solid line, and the pressure side by a dashed line. The C_p plot for the case of the metal foams shows an interesting shape close to the transition from porous to solid. There is a sharp decrease in the coefficient in pressure for both cases, however the decrease is seen to be larger in the more porous case. The decrease in pressure coefficient at this point could suggest a small separation region, as the shape is similar to the C_p distribution of a bluff body or forward facing step [36]. Beyond 30% of the chord and further to the trailing edge the pressure coefficient for all cases collapse on top of each other. In the case of the additive manufactured leading edges P7 and P8, they show a good agreement for all of the measured area on the solid part of the airfoil. There is a small increase for the P8 case, but it is not of the same scale in the case of the metal foams. Figures 13c and 13d display the $C_{p_{rms}}$ values and show an interesting trend. For all cases, including the solid leading edge, the suction side experiences a larger fluctuation in the value of pressure coefficient compared to the pressure side, although the overall shape remains similar. For the metal foams cases, there is a great increase in the rms value, and the suction side for both P1 and P2 at the start of the solid part of the airfoil.

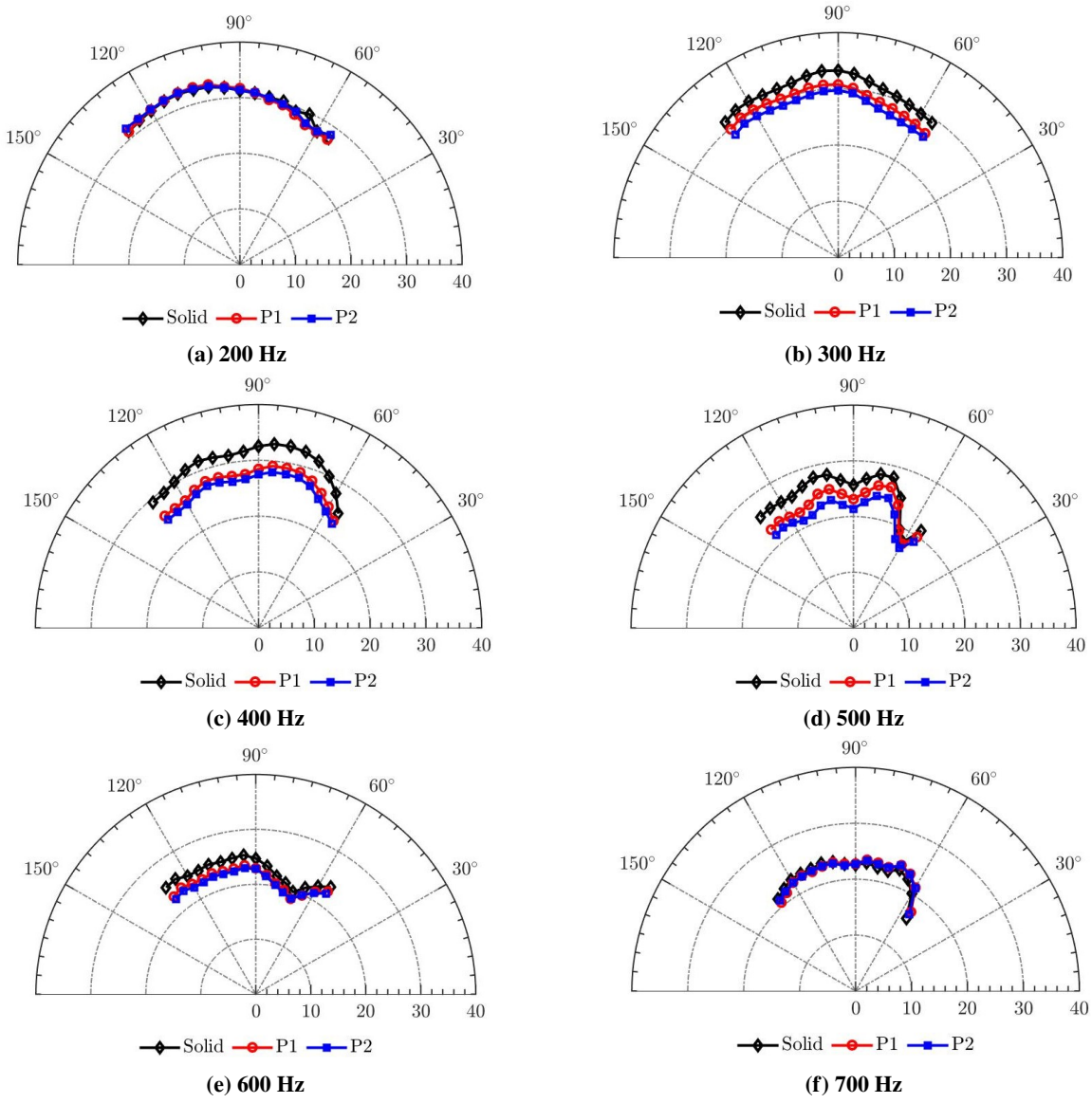

(a) 200 Hz **(b) 300 Hz**

(c) 400 Hz **(d) 500 Hz**

(e) 600 Hz **(f) 700 Hz**

Fig. 11 Directivity of the power spectral density of the radiated sound by the metal foam leading edges and the solid baseline for selected frequencies.

Contrary to the C_p data, both the P1 and P2 match well for their values with the exception of $x/C = 0.18$ where the P1 does not decrease at the same rate as P2. This is resolved by $x/C = 0.24$ where both P1 and P2 follow the same trend for the rest of the chord of the airfoil. The tailored surface leading edges also show an increase at the start of the solid part of the airfoil, however the increase is not of the same magnitude as the metal foams. Overall P7 and P8 have a good agreement with the solid case beyond $x/C = 0.18$ to the trailing edge, with the exception of a matching peak in both P7 and P8 between $x/C = 0.6$ and $x/C = 0.7$. P1 and P2 have a hump at the same location but it has a lower magnitude, but there is no change in pressure coefficient at this location for any case. Overall it appears that P7 and P8 perform more in line with the baseline for the solid part of the airfoil, however as the porous part of the leading edge is not instrumented it is not possible to make comment on the overall aerodynamic performance. To gain more information on this, either the porous leading edge must be instrumented in a non-intrusive manner, or force balance testing is required.

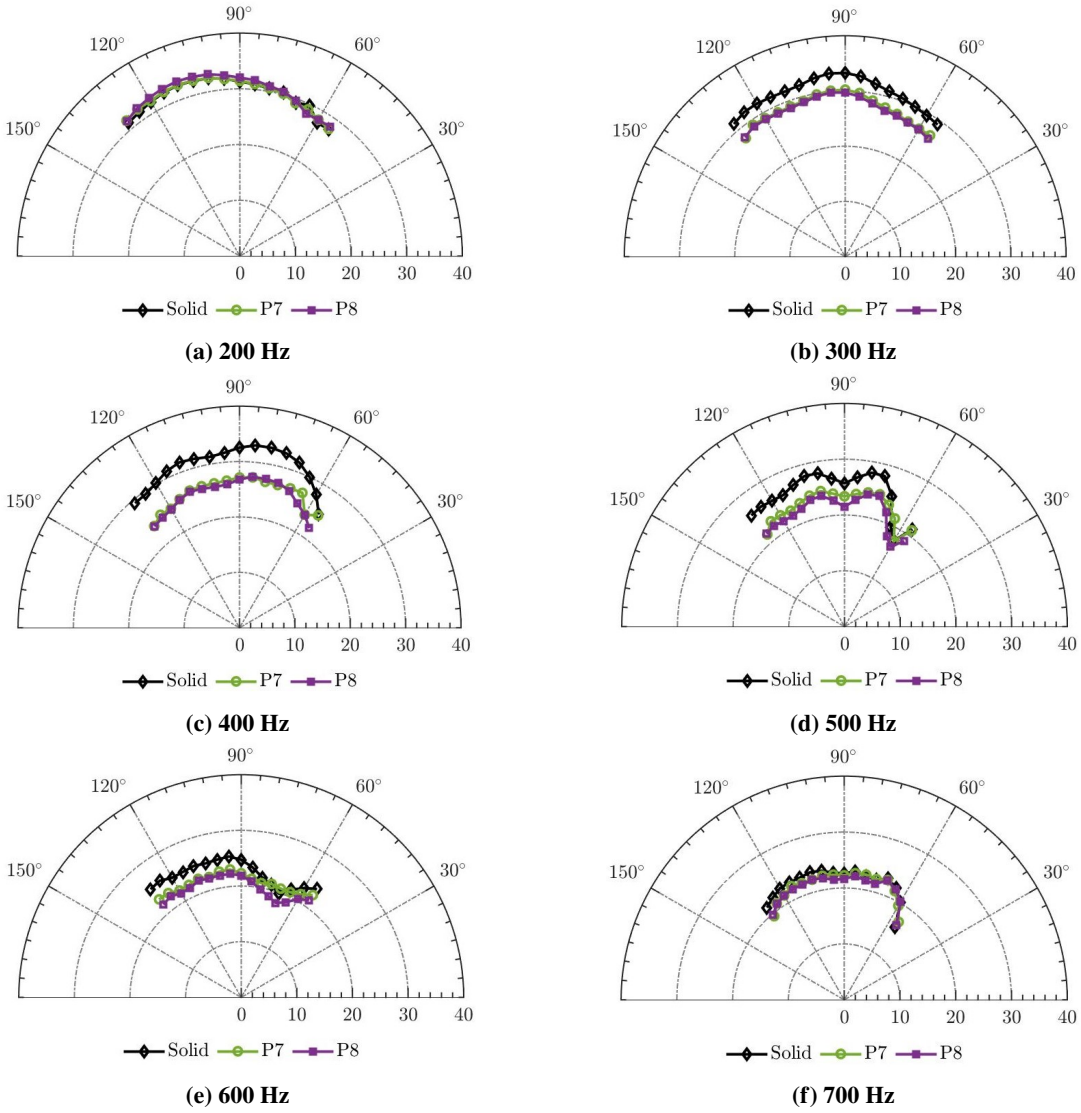

(a) 200 Hz **(b) 300 Hz**

(c) 400 Hz **(d) 500 Hz**

(e) 600 Hz **(f) 700 Hz**

Fig. 12 Directivity of the power spectral density of the radiated sound by the tailored structures leading edges and the solid baseline for selected frequencies.

V. Conclusion

Leading edge interaction noise and how it is affected by the introduction of porous leading edges has been studied. The study comprised of an instrumented solid leading edge, metal foam leading edges, and mathematically defined porous, 3D printed structures. It was found, as with previous studies, that the introduction of metal foam leading edges reduce the low frequency content of the noise by 2-3dB, but incurs a higher frequency penalty above 1000 Hz. The additive manufactured leading edges showed a more promising noise reduction, but a larger increase at high frequency. However, because the high frequency contribution to the overall sound is much lower than the low frequency contribution, this resulted in an overall noise reduction greater than that of the metal foam leading edges. The most effective overall sound reduction came from the covered Schwarz-P surface which was over 5 dB at certain frequencies and, at low angles of attack, the coefficient of pressure gave a good match to the solid case between $x/C = 0.1$ and $x/C = 1$. The overall sound pressure level directivity appears to be similar across all of the samples tested. Furthermore, a significantly higher reduction in overall sound pressure level for polar angles above 70 is reported. To further assess the benefits of the porous materials in aeroacoustic applications, further aerodynamic testing is required for the quantification of the flow field around the leading edge.

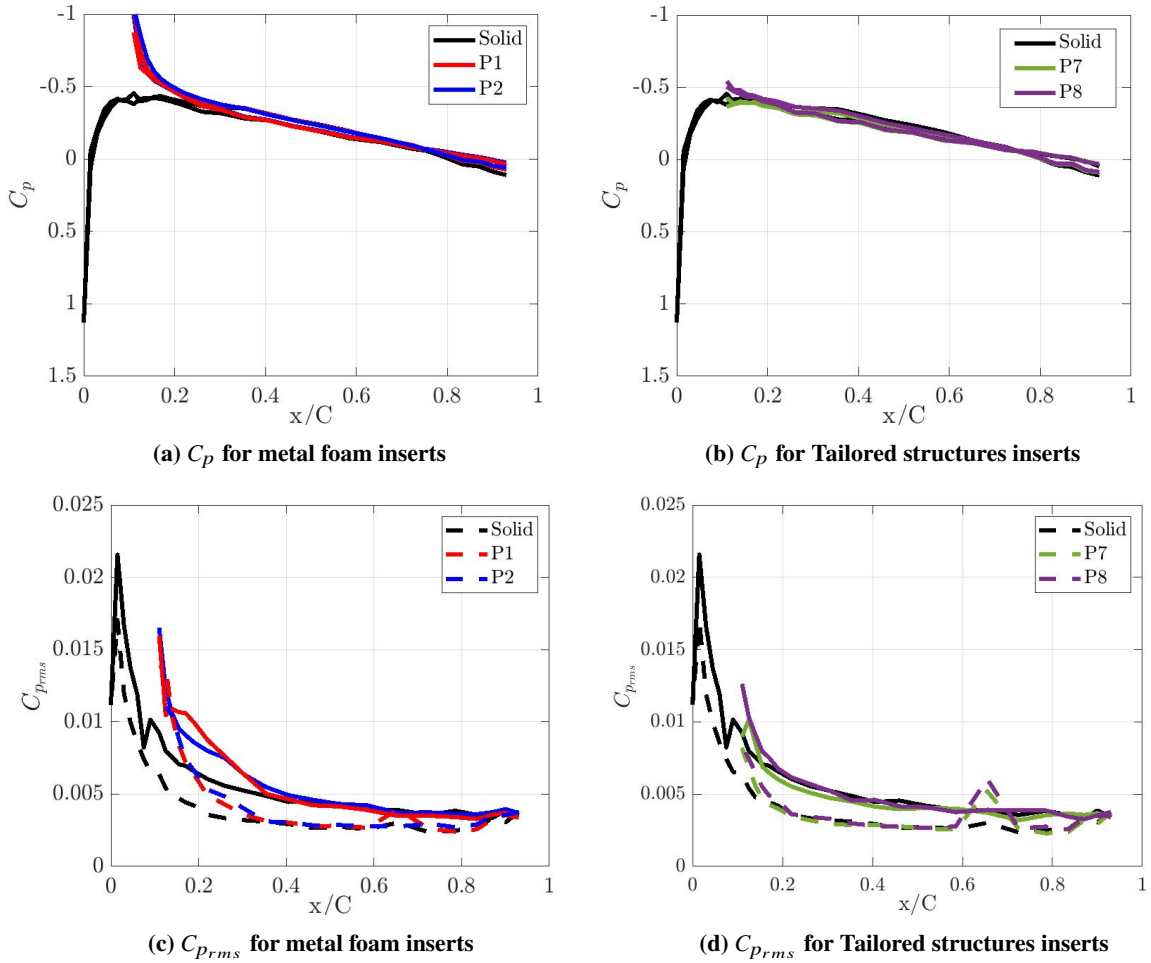

(a) C_p for metal foam inserts

(b) C_p for Tailored structures inserts

(c) $C_{p_{rms}}$ for metal foam inserts

(d) $C_{p_{rms}}$ for Tailored structures inserts

Fig. 13 Coefficient of pressure and rms values P1 and P2, and P7 and P8 leading edges and the comparison to the solid baseline.

Acknowledgments

The authors would like to acknowledge the financial support of Embraer S.A. and EPSRC.

References

[1] Paterson, R., and Amiet, R., *Acoustic radiation and surface pressure characteristics of an airfoil due to incident turbulence*, chapter and pages. https://doi.org/10.2514/6.1976-571.

[2] Amiet, R., "Acoustic radiation from an airfoil in a turbulent stream," *Journal of Sound and Vibration*, Vol. 41, No. 4, 1975, pp. 407 – 420. https://doi.org/https://doi.org/10.1016/S0022-460X(75)80105-2.

[3] Moreau, S., and Roger, M., *Effect of Angle of Attack and Airfoil Shape on Turbulence-Interaction Noise*, chapter and pages. https://doi.org/10.2514/6.2005-2973.

[4] Devenport, W. J., Staubs, J. K., and Glegg, S. A., "Sound radiation from real airfoils in turbulence," *Journal of Sound and Vibration*, Vol. 329, No. 17, 2010, pp. 3470 – 3483. https://doi.org/https://doi.org/10.1016/j.jsv.2010.02.022.

[5] Hutcheson, F. V., Brooks, T. F., and Stead, D. J., "Measurement of the Noise Resulting from the Interaction of Turbulence with a Lifting Surface," *International Journal of Aeroacoustics*, Vol. 11, No. 5-6, 2012, pp. 675–700. https://doi.org/10.1260/1475-472X.11.5-6.675.

[6] Gill, J., Zhang, X., and Joseph, P., "Symmetric airfoil geometry effects on leading edge noise," *The Journal of the Acoustical Society of America*, Vol. 134, No. 4, 2013, pp. 2669–2680. https://doi.org/10.1121/1.4818769.

[7] Gill, J. R., Zhang, X., and Joseph, P., *Effects of Real Airfoil Geometry on Leading Edge Gust Interaction Noise*, chapter and pages. https://doi.org/10.2514/6.2013-2203.

[8] Gershfeld, J., "Leading edge noise from thick foils in turbulent flows," *The Journal of the Acoustical Society of America*, Vol. 116, No. 3, 2004, pp. 1416–1426. https://doi.org/10.1121/1.1780575.

[9] Szoke, M., and Azarpeyvand, M., "Active Flow Control Methods for the Reduction of Trailing Edge Noise," Proceedings of the 23rd AIAA/CEAS Aeroacoustics Conference, Denver, CO, AIAA 2017-3004.

[10] Szőke, M., Fiscaletti, D., and Azarpeyvand, M., "Effect of inclined transverse jets on trailing-edge noise generation," *Physics of Fluids*, Vol. 30, No. 8, 2018, p. 085110.

[11] Showkat Ali, S. A., Azarpeyvand, M., and Ilário da Silva, C. R., "Trailing-edge flow and noise control using porous treatments," *Journal of Fluid Mechanics*, Vol. 850, 2018, pp. 83–119. https://doi.org/10.1017/jfm.2018.430.

[12] Showkat Ali, S. A., Azarpeyvand, M., Szőke, M., and Ilário da Silva, C. R., "Boundary layer flow interaction with a permeable wall," *Physics of Fluids*, Vol. 30, No. 8, 2018, p. 085111. https://doi.org/10.1063/1.5043276.

[13] Showkat Ali, S. A., Azarpeyvand, M., and da Silva], C. R. I., "Trailing edge bluntness noise reduction using porous treatments," *Journal of Sound and Vibration*, Vol. 474, 2020, p. 115257. https://doi.org/https://doi.org/10.1016/j.jsv.2020.115257.

[14] Liu, X., Jawahar, H. K., Azarpeyvand, M., and Theunissen, R., "Aerodynamic Performance and Wake Development of Airfoils with Serrated Trailing-Edges," *AIAA Journal*, Vol. 55, No. 11, 2017, pp. 3669–3680.

[15] Mayer, Y. D., Lyu, B., Jawahar, H. K., and Azarpeyvand, M., "A semi-analytical noise prediction model for airfoils with serrated trailing edges," *Renewable Energy*, Vol. 143, 2019, pp. 679 – 691. https://doi.org/https://doi.org/10.1016/j.renene.2019.04.132.

[16] Jawahar], H. K., Ai, Q., and Azarpeyvand, M., "Experimental and numerical investigation of aerodynamic performance for airfoils with morphed trailing edges," *Renewable Energy*, Vol. 127, 2018, pp. 355 – 367. https://doi.org/https://doi.org/10.1016/j.renene.2018.04.066.

[17] Lyu, B., Azarpeyvand, M., and Sinayoko, S., *Noise Prediction for Serrated Leading-edges*, chapter and pages. https://doi.org/10.2514/6.2016-2740, URL https://arc.aiaa.org/doi/abs/10.2514/6.2016-2740.

[18] Lyu, B., and Azarpeyvand, M., "On the noise prediction for serrated leading edges," *Journal of Fluid Mechanics*, Vol. 826, 2017, p. 205–234. https://doi.org/10.1017/jfm.2017.429.

[19] Kim, J., Haeri, S., and Joseph, P., "On the reduction of aerofoil-turbulence interaction noise associated with wavy leading edges," *Journal of Fluid Mechanics*, Vol. 792, 2016, pp. 526–552. Data files are made available from http://dx.doi.org/10.5258/SOTON/397245 as required by EPSRC Research Data Policy.

[20] Narayanan, S., Chaitanya, P., Haeri, S., Joseph, P., Kim, J. W., and Polacsek, C., "Airfoil noise reductions through leading edge serrations," *Physics of Fluids*, Vol. 27, No. 2, 2015, p. 025109. https://doi.org/10.1063/1.4907798.

[21] Chaitanya, P., Joseph, P., Narayanan, S., Vanderwel, C., Turner, J., Kim, J. W., and Ganapathisubramani, B., "Performance and mechanism of sinusoidal leading edge serrations for the reduction of turbulenceaerofoil interaction noise," *Journal of Fluid Mechanics*, Vol. 818, 2017, pp. 435–464. https://doi.org/10.1017/jfm.2017.141.

[22] Roger, M., Schram, C., and Santana, L. D., *Reduction of Airfoil Turbulence-Impingement Noise by Means of Leading-Edge Serrations and/or Porous Material*, chapter and pages. https://doi.org/10.2514/6.2013-2108.

[23] Roger, M., and Moreau, S., "Airfoil Turbulence-Impingement Noise Reduction by Porosity or Wavy Leading-Edge Cut : Experimental Investigations," 2016.

[24] Geyer, T., Sarradj, E., Giesler, J., and Hobracht, M., *Experimental assessment of the noise generated at the leading edge of porous airfoils using microphone array techniques*, chapter and pages. https://doi.org/10.2514/6.2011-2713.

[25] Geyer, T., Sarradj, E., and Giesler, J., "Application of a Beamforming Technique to the Measurement of Airfoil Leading Edge Noise," *Advances in Acoustics and Vibration*, Vol. 2012, 2012, pp. 1–16. https://doi.org/10.1155/2012/905461.

[26] Sarradj, E., and Geyer, T., *Noise Generation by Porous Airfoils*, chapter and pages. https://doi.org/10.2514/6.2007-3719.

[27] Geyer, T. F., Lucius, A., Schrödter, M., Schneider, M., and Sarradj, E., "Reduction of Turbulence Interaction Noise Through Airfoils With Perforated Leading Edges," *Acta Acustica united with Acustica*, Vol. 105, No. 1, 2019, pp. 109–122. https://doi.org/doi:10.3813/AAA.919292.

[28] Roger, M., Schram, C., and Santana, L. D., *Reduction of Airfoil Turbulence-Impingement Noise by Means of Leading-Edge Serrations and/or Porous Material*, chapter and pages. https://doi.org/10.2514/6.2013-2108.

[29] Carpio, A. R., Avallone, F., and Ragni, D., *On the Role of the Flow Permeability of Metal Foams on Trailing Edge Noise Reduction*, chapter and pages. https://doi.org/10.2514/6.2018-2964.

[30] Sinnige, T., Corte, B. D., De Vries, R., Avallone, F., Merino-Martínez, R., Ragni, D., Eitelberg, G., and Veldhuis, L. L. M., "Alleviation of Propeller-Slipstream-Induced Unsteady Pylon Loading by a Flow-Permeable Leading Edge," *Journal of Aircraft*, Vol. 56, No. 3, 2019, pp. 1214–1230. https://doi.org/10.2514/1.C035250.

[31] Zamponi, R., de Wyer, N. V., and Schram, C. F., *Experimental Investigation of Airfoil Turbulence-Impingement Noise Reduction Using Porous Treatment*, chapter and pages. https://doi.org/10.2514/6.2019-2649.

[32] Mayer, Y. D., Jawahar, H. K., Szőke, M., Ali, S. A. S., and Azarpeyvand, M., "Design and performance of an aeroacoustic wind tunnel facility at the University of Bristol," *Applied Acoustics*, Vol. 155, 2019, pp. 358 – 370. https://doi.org/https://doi.org/10.1016/j.apacoust.2019.06.005.

[33] Mayer, Y., Zang, B., and Azarpeyvand, M., "Near-field aeroacoustic characteristics of a stalled NACA 0012 aerofoil," *Proceedings of the 23rd International Congress on Acoustics, integrating 4th EAA Euroregio 2019*, edited by M. Ochmann, DEGA e.V., 2019, pp. 5421–5428.

[34] Schwarz, H. A., *Gesammelte mathematische abhandlungen*, Vol. 260, American Mathematical Soc., 1972.

[35] Neovius, E. R., "Bestimmung zweier speciellen periodischen Minimalflächen, auf welchen unendlich viele gerade Linien und unendlich viele ebene geodätische Linien liegen," 1883.

[36] Khalighi, B., Chen, K.-H., and Iaccarino, G., "Unsteady Aerodynamic Flow Investigation Around a Simplified Square-Back Road Vehicle With Drag Reduction Devices," *Journal of Fluids Engineering*, Vol. 134, No. 6, 2012. https://doi.org/10.1115/1.4006643.